Electronic Supplementary Information

AuIr alloy with arbitrarily adjustable lattice parameters as a highly efficient electrocatalyst for the oxygen reduction reaction

Conghui Zhai, Ruoxi Ming, Hanruo Chen, Lingjun Tan, Ning Cong, Juanjuan Han, Xiaorong Zhou, Xiaohong Yang, Zhandong Ren* and Yuchan Zhu*

School of Chemical and Environmental Engineering, Wuhan Polytechnic University, Wuhan, 430023, P. R. China.

* Corresponding author:

Zhandong Ren, Professor, School of Chemical and Environmental Engineering, Wuhan Polytechnic University, Wuhan, 430023, P. R. China.

E-mail: renzhandong@163.com. Tel.: 86-27-83943956.

Yuchan Zhu, Professor, School of Chemical and Environmental Engineering, Wuhan Polytechnic University, Wuhan, 430023, P. R. China.

E-mail: zhuyuchan@163.com. Tel.: 86-27-83943956.

Experimental methods

Preparation of Au, AuIr alloys, Ir and Pt

AuIr alloy was prepared by magnetron sputtering in TRP-450 magnetron sputtering instrument (SKY Technology Development Co. Ltd.). The purity of Au and Ir sputtering target is 99.99% (Beijing Goodwill Metal Co. Ltd.). The carrier is a glass slide (Citotest Scientific), which is ultrasonically cleaned by acetone, water and ethanol and then transferred into a vacuum chamber. Before sputtering, the vacuum chamber was evacuated to 4×10^{-4} Pa with turbo pump (HiPace® 700, Pfeiffer vacuum). Then, high purity argon gas (99.999%) was continuously introduced at the flow rate of 100 sccm for 10 min to further remove the air in the vacuum chamber. Next, the vacuum pressure was adjusted to 1.0 Pa.

During sputtering, a DC power supply is used for ionization, and a negative bias voltage is applied to the cathode target, so that Ar gas is ionized into Ar^+. Ar^+ generated in the discharge process are accelerated to bombard the target surface under the action of the high-energy electric field in the plasma sheath on the cathode target surface. On the one hand, the bombardment of high-energy sputtering gas ions on the target surface causes some atoms on the target surface to obtain recoil energy and leave the target surface to become sputtering atoms and finally deposit on the substrate surface. On the other hand, secondary electrons are emitted from the target surface and accelerated into the glow discharge plasma area under the action of the cathode target sheath. The secondary electrons in the plasma are bound by the magnetic field on the target surface and ionized by the collision with the sputtering gas atoms, thus the magnetron discharge becomes self-sustaining. In this experiment, when Au and Ir are sputtered at the same time, Au and Ir sputtering atoms will collide violently and react with each other in the process of flying to the matrix at high speed, thus forming the alloy structure. Au and Ir sputtered atoms have high energy, which can collide effectively and easily form alloy structure, and are not limited by composition. As shown in Table S1, the sputtering speed of Au and Ir can be controlled by controlling the sputtering power of DC power supply, so as to control the ratio of Au and Ir in the alloy. In addition, by controlling the sputtering time, the loading capacity of the alloy can be controlled. Magnetron sputtering of Au and Ir is the same as that of AuIr alloy, except that Au target or Ir target is used alone for sputtering. The magnetron sputtering preparation of Pt is the same as that of AuIr alloy, except that Pt target (99.99%) is used to replace it.

When sputtered atoms reach the substrate surface, their initial positions are random and disordered. Sputtering atoms adsorbed on the substrate surface become adatom and transiently migrate on the substrate surface. In the process of surface migration, on the one hand, the adatoms exchange energy with the substrate atoms to reduce their energy to below the desorption energy. On the one hand, the surface energy of the system is minimized as much as possible. When the concentration of adatoms on the substrate surface reaches a certain level, the adjacent adatoms aggregate into a steady-state atomic island. Atomic islands grow up and merge in the form of atomic stacks, thus forming a continuous structure on the substrate surface. The migration, diffusion and nucleation of atoms on the substrate surface determine the growth mode.

Materials characterization

X-ray diffraction (XRD) patterns were acquired on an XRD-7000 X-ray diffractometer (Shimadzu, Japan). Transmission Electron Microscopy (TEM) were conducted on an JEM-2100F (JEOL, Japan). Scanning Electron Microscope (SEM) images were taken with a ΣIGMA field-emission

SEM (Zeiss, Germany). X-ray photoelectron spectrometry (XPS: ESCLAB 250Xi, Thermo Fisher Scientific, The United States) with monochromatized Al Kα radiation was used to analyze the electronic properties. Analysis of the composition of the electrode was carried out by X-ray fluorescence (XRF: EDX-7000, Shimadzu, Japan).

Electrochemical measurements

In the three-electrode electrochemical cell, the electrochemical experiment was carried out with carbon paper (CP) as the counter electrode and Hg/HgO/KOH (1.0 mol L^{-1}) as the reference electrode. The preparation process of working electrode is as follows. 2.5 mg AuIr (Au, Ir) or 2.0 mg Pt was ultrasonically removed from the slide for 24 h to ethanol solution to obtain an ethanol dispersion solution of AuIr (Au, Ir) or Pt. Then 2.5 mg or 3.0 mg XC-72 carbon powder was added into the ethanol dispersion solution, and stirring and ultrasound were alternately performed for 24 h. Next, 50 wt% AuIr/C (Au/C, Ir/C) or 40 wt% Pt/C sample was obtained by vacuum drying at 40 ℃ for 12 h. 5 mg of AuIr/C (Au/C, Ir/C) or Pt/C was dispersed into 1 mL 0.05 wt% Nafion/ethanol solution, and the ultrasonic dispersion was carried out for 30 min to make it uniformly dispersed. 20 μL were taken from the dispersion and dropped on a glassy carbon electrode with a diameter of 5 mm, and the working electrode was obtained after drying. The loading of AuIr (Au, Ir) working electrode is 0.255 mg cm^{-2}. The loading of Pt working electrode is 0.204 mg cm^{-2}.

Cyclic voltammetry (CV) measurements were performed at a scanning rate of 100 mV s^{-1} in 1.0 M KOH solution saturated with Ar gas. The electrochemical surface areas (ECSAs) were obtained as follows. First, the CV scanning in the double-layer at different scanning speeds (5, 10, 15, 20, 30, 40, 50, 60, 80, 100 mV s^{-1}) is performed to obtain the double-layer current at different scanning speeds (the average value of the current at the dotted line in Fig. S8). Then, the linear relationship between scanning speed (v) and double-layer current (j) is obtained by plotting (Fig. S9). Next, the slope in j-v curve is the double-layer capacitance (C_d), which can be divided by the reference value of capacity per the unit area (C_{ref}, 91 μF cm^{-2} in 1.0 M KOH) to obtain ECSA. The value of C_{ref} in 1.0 M KOH can be preliminarily calibrated through ECSA obtained by the method of underpotential deposition (UPD) of Cu on Au electrode surface in 1.0 mM $CuSO_4$ and 0.1 M H_2SO_4 solution. At first, the ECSA of Au is obtained by Cu UPD method. According to Fig. S19, the potential of Cu monolayer adsorption is 0.26 V, and its stripping charge (Q) is 1.35 mC. Therefore, the ECSA is 3.21 cm^2 (ECSA = Q / Q_{ML} = 1.35 mC / 0.42 mC cm^{-2}= 3.21 cm^2). Then, in Fig. S20, the double-layer capacitance (C_d) of Au electrode in 1.0 M KOH solution is 0.292 mF. So, the value of C_{ref} is 91 μF cm^{-2} (C_{ref} = C_d / ECSA = 0.292 mF / 3.21 cm^2 = 91 μF cm^{-2}).

The oxygen reduction reaction (ORR) polarization curves were obtained by sweeping at a scan rate of 5 mV s^{-1} with the different rotation rate (100, 400, 625, 900, 1225, 1600, 2025, 2500 rpm) in O_2-saturated 1.0 M KOH. The following equations (Koutecky-Levich, KL) were used for the calculation of the kinetic current and electron transfer number (n).

$$j^{-1} = j_k^{-1} + j_d^{-1} = j_k^{-1} + (B\omega^{1/2})^{-1}$$

$$B = 0.62nFC_0D_0^{2/3}v^{-1/6}$$

where j is the actual current density, j_k and j_d are the kinetic- and diffusion-limiting current densities, respectively, B is the slope, ω is the angular velocity of rotating disk electrode system (RDE, MSR, Pine, The United States), n is the electron transfer number, F is the Faraday constant (96485 C mol^{-1}), C_0 is the bulk concentration of O_2 (0.84×10^{-6} mol cm^{-3}), D_0 denotes the diffusion

coeffcient of O_2 (1.85×10^{-5} cm^2 s^{-1}), and v represents the kinetic viscosity of the electrolyte (0.0106 cm^2 s^{-1}) in 1.0 M KOH aqueous solution.

DFT calculations

First-principles calculations were performed using the Vienna Ab Initio Simulation Package (VASP, version 5.3) within a PBE (Perdew Burke Ernzerhof) generalized gradient approximation (GGA) to the exchange and correlation functional. A projector augmented wave (PAW) basis along with a plane-wave kinetic energy cutoff of 408 eV was employed for all computations. During the geometry optimization, the adsorbate layer and the top three layers of the slab were allowed to relax. The energies were converged to 1×10^{-3} eV per atom and ionic relaxations were allowed until the absolute value of force on each atom was below 0.02 eV/A. $AE_O = E(O/M) – E(M) - 1/2E(O_2)$, such that the negative value indicates the dissociation of O_2 on the studied surface being thermodynamically spontaneous, whereas the positive means the opposite.

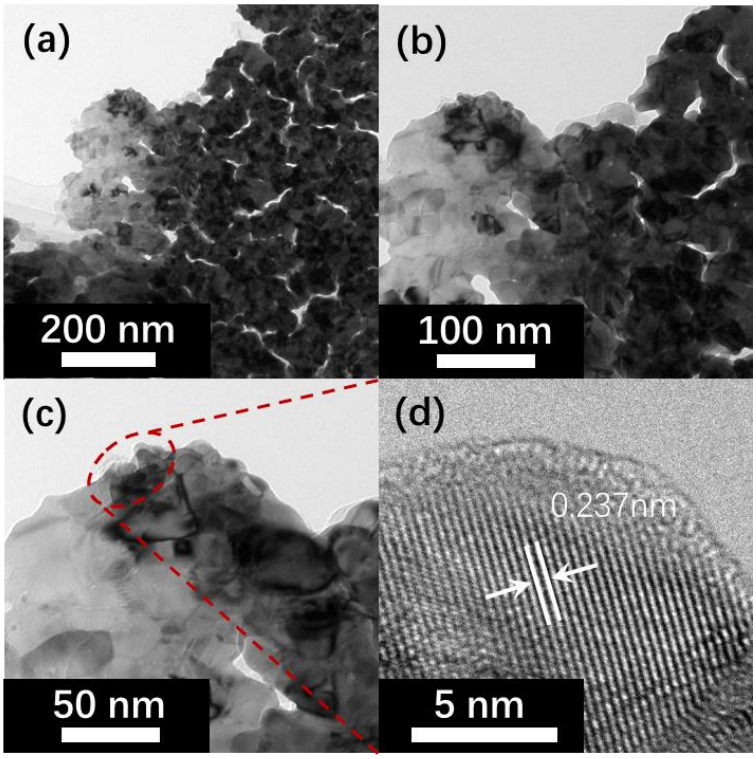

Figure S1 TEM and HRTEM images of Au nanosheets.

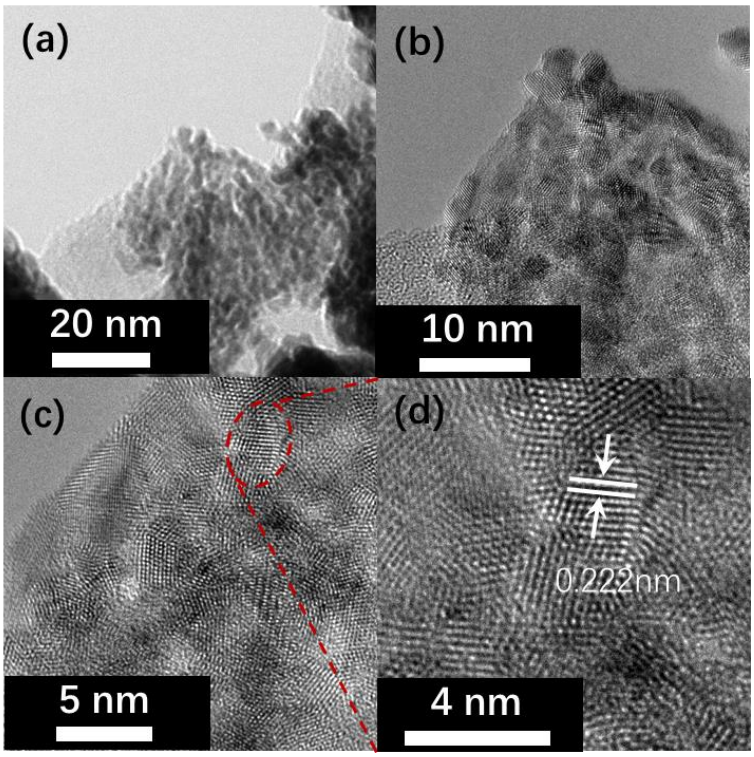

Figure S2 TEM and HRTEM images of Ir nanoparticles.

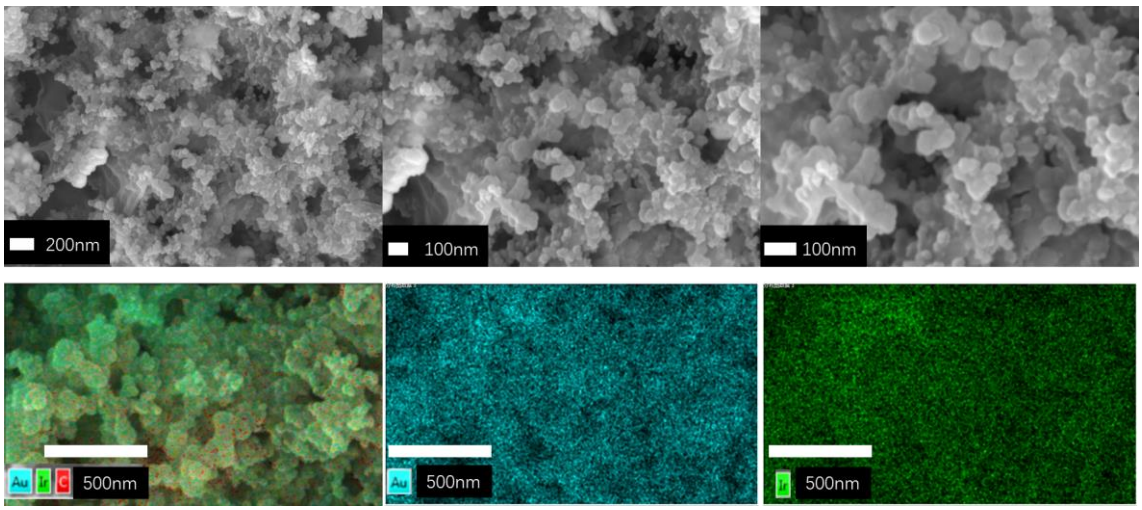

Figure S3 SEM and element mapping images of Au_5Ir_5 alloy nanoparticles.

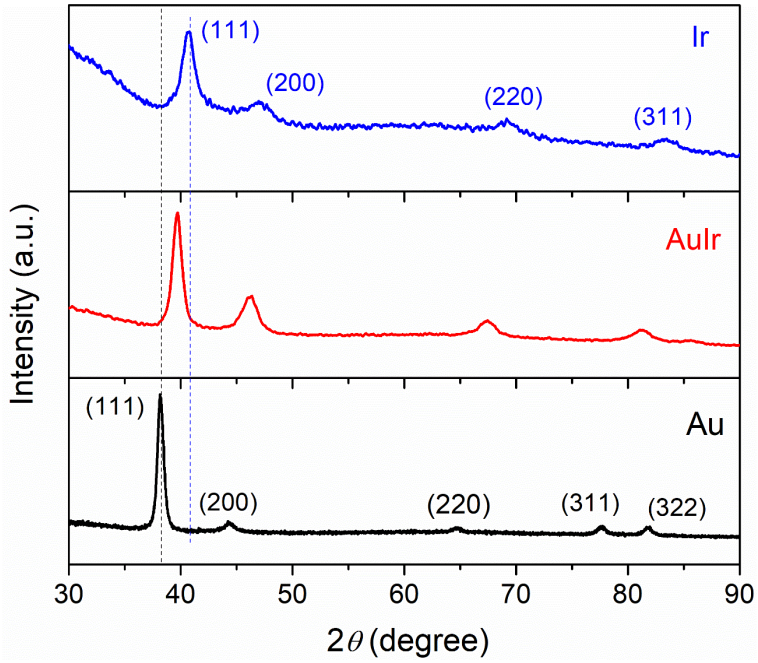

Figure S4 The XRD patterns of Au nanosheets, Au_5Ir_5 alloy nanoparticles and Ir nanoparticles.

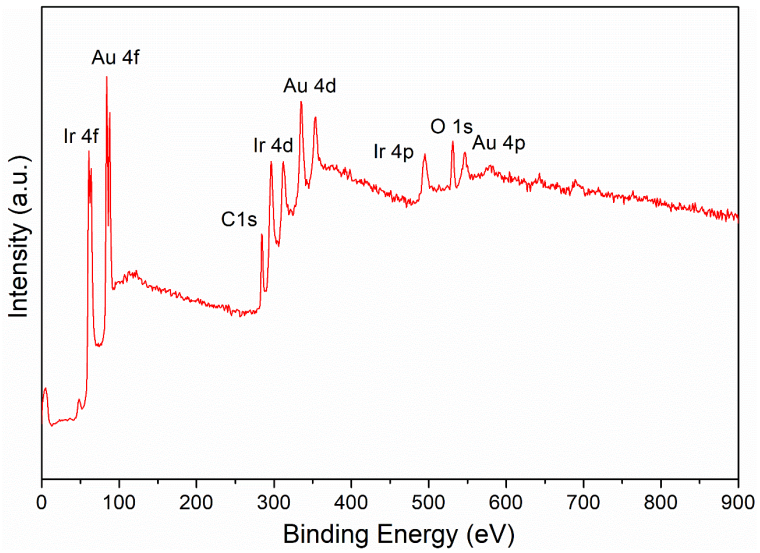

Figure S5 The XPS survey spectrum of Au_5Ir_5 alloy nanoparticles.

As presented in Fig. 2e, the peaks at 88.0 and 84.4 eV can be attributed to the spin splitting peaks of the Au $4f_{7/2}$ and $4f_{5/2}$ orbitals of Au^0. However, compared with pure Au (87.7 and 84.0 eV), the core-level spectra of Au 4f in Au_5Ir_5 alloy is also positively shifted to a higher value by 0.4-0.6 eV. This seems to contradict the previous analysis (Electron transfer from Ir to Au). The reason for this is that although the number of Au 6s electrons (conduction electrons) increases, the number of Au 5d electrons (localization electrons) decreases. Furthermore, the shielding effect of Au 5d electrons on the nuclei is stronger than that of Au 6s electrons, which leads to a positive shift in the binding energy of Au 4f in the alloy.

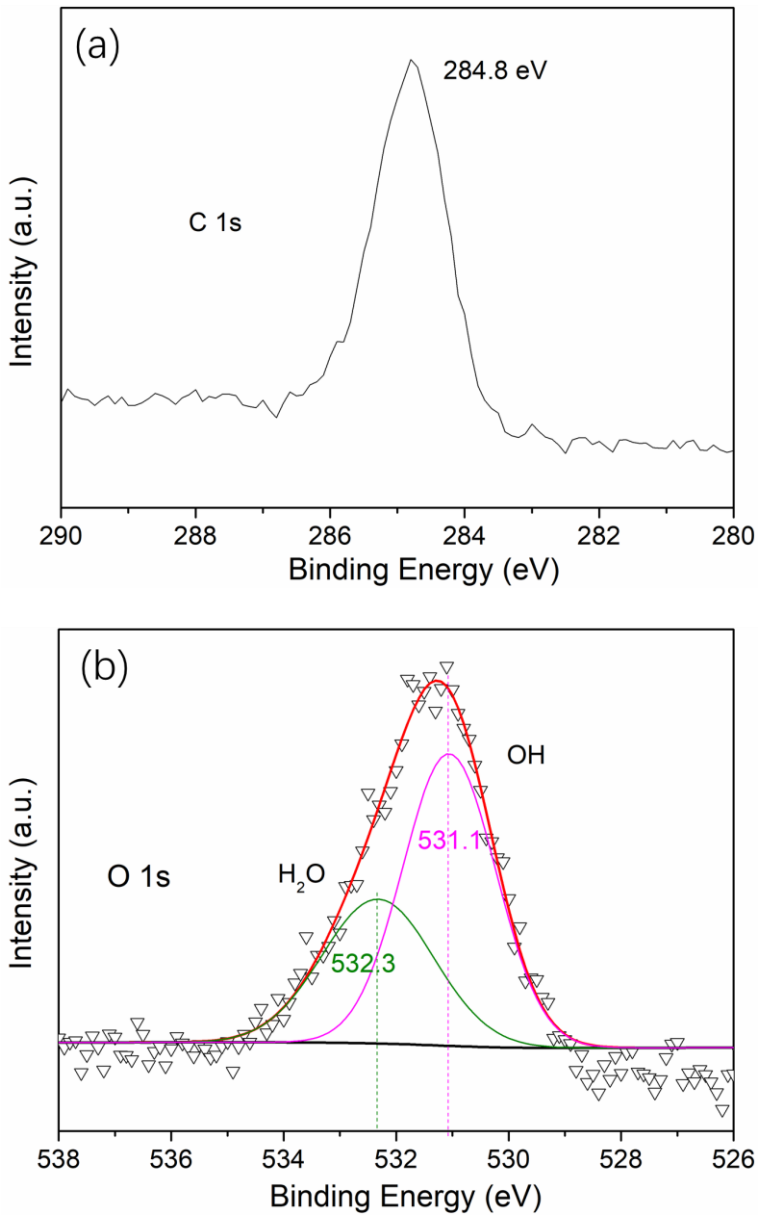

Figure S6 The XPS core-level spectrum of C 1s (a) and O 1s (b) of Au_5Ir_5 alloy nanoparticles.

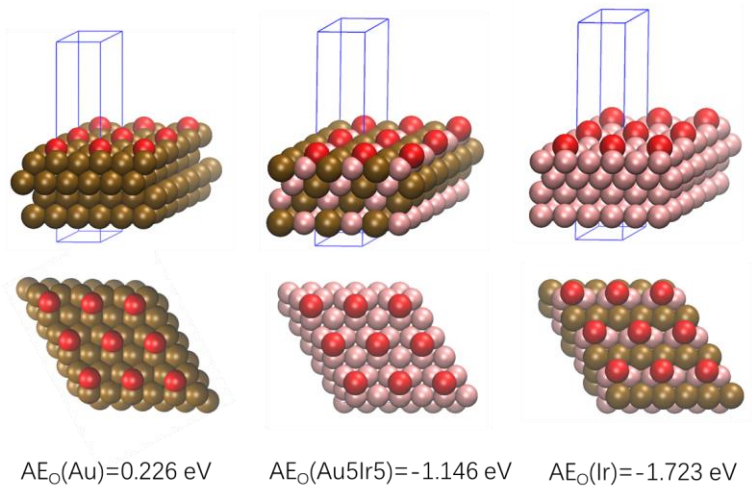

Figure S7 DFT calculations of AE_O for Au, Au_5Ir_5 alloy and Ir.

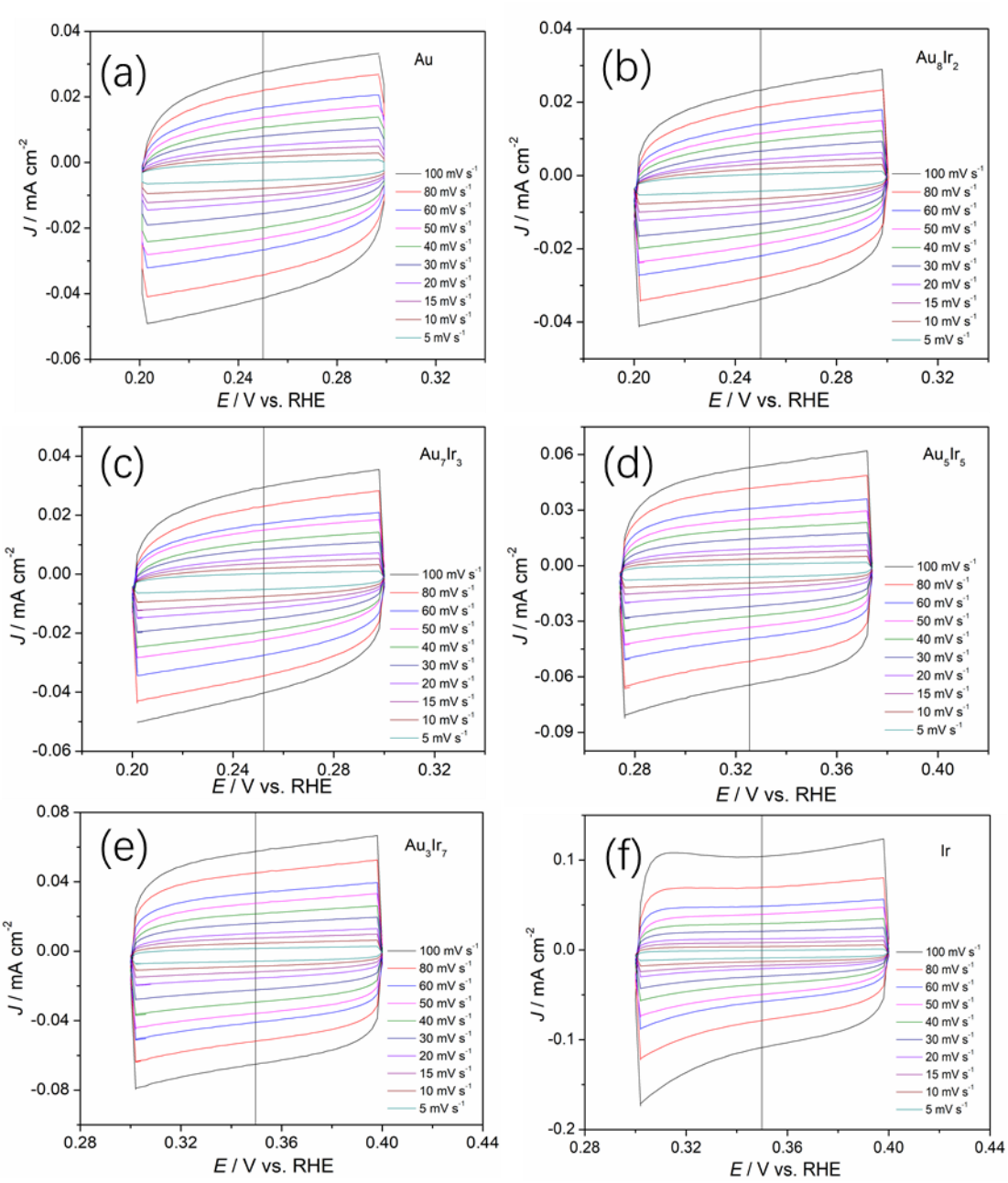

Figure S8 The double layer at different scanning speeds of AuIr alloys with different proportions (a) Au, (b) Au_8Ir_2, (c) Au_7Ir_3, (d) Au_5Ir_5, (e) Au_3Ir_7, (f) Ir.

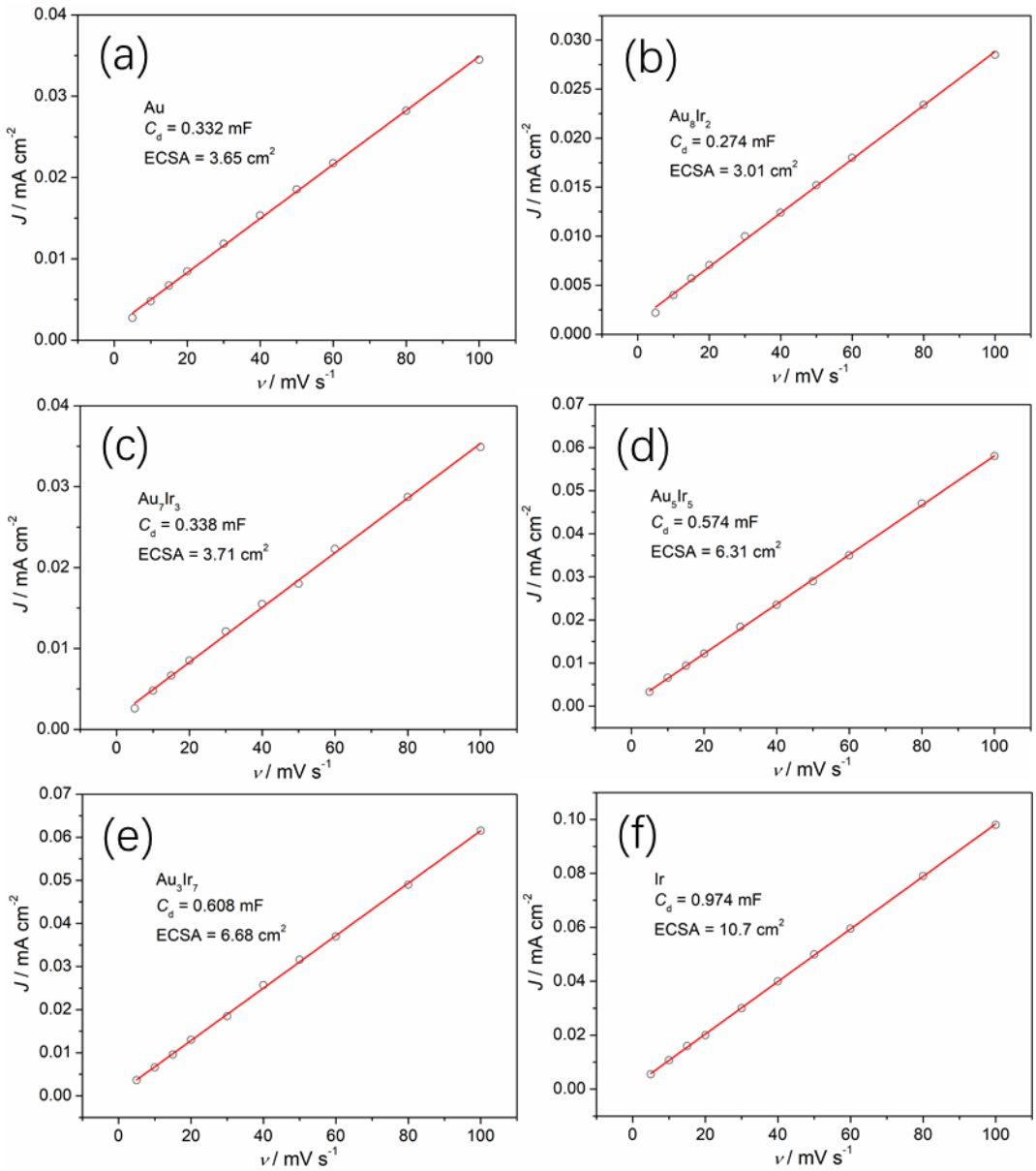

Figure S9 The *j*-*v* curve of AuIr alloys with different proportions (a) Au, (b) Au_8Ir_2, (c) Au_7Ir_3, (d) Au_5Ir_5, (e) Au_3Ir_7, (f) Ir.

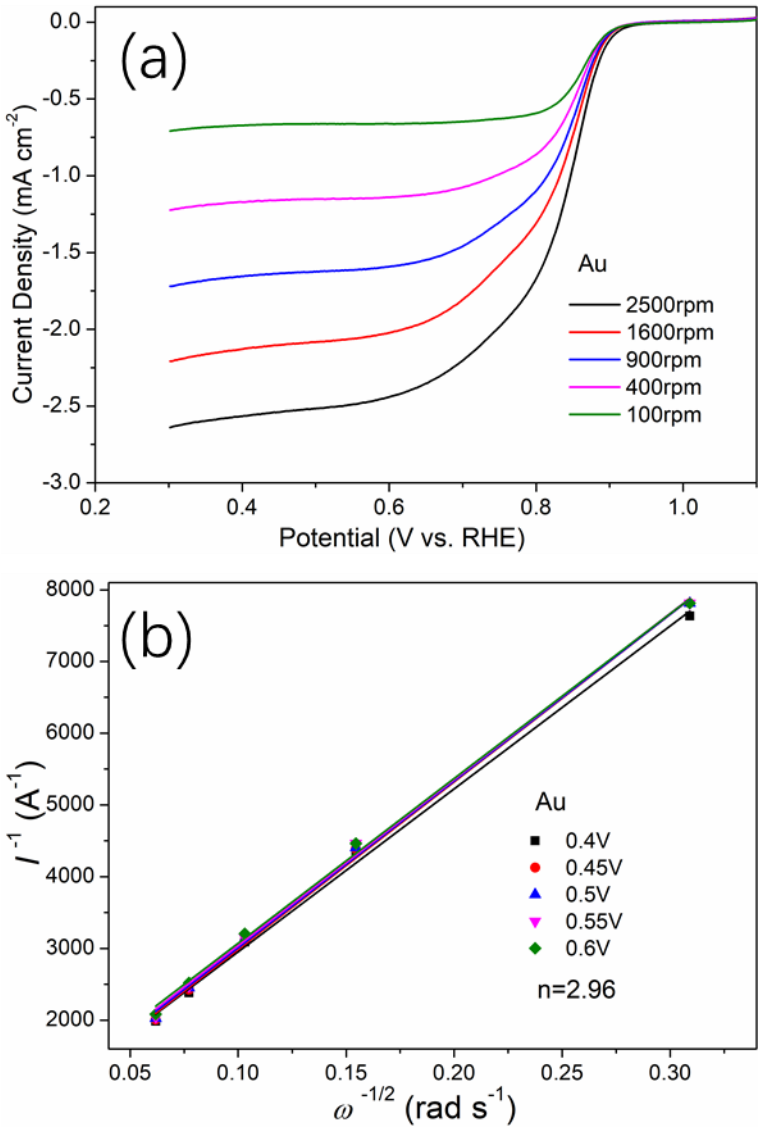

Figure S10 ORR activities at different rotate speeds (a) and transfer electron number (n) under different potential (b) of Au.

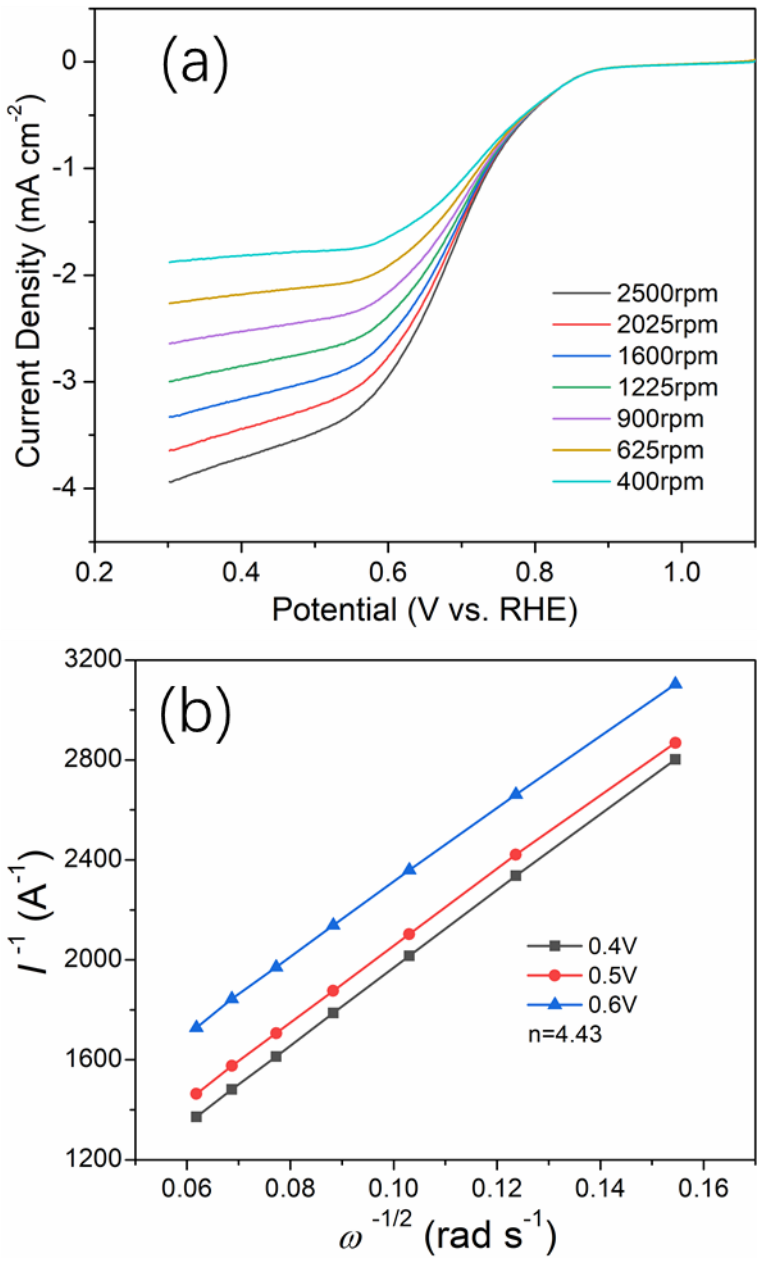

Figure S11 ORR activities at different rotate speeds (a) and transfer electron number (n) under different potential (b) of Ir.

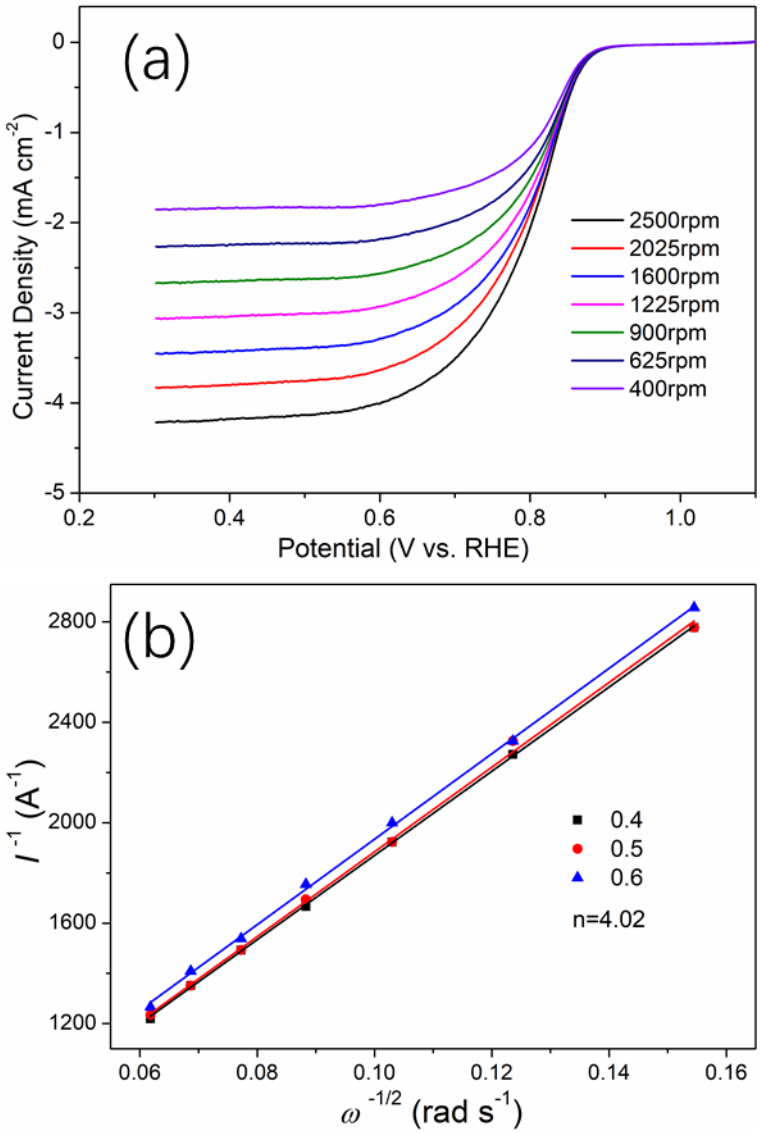

Figure S12 ORR activities at different rotate speeds (a) and transfer electron number (n) under different potential (b) of Au_5Ir_5 alloy.

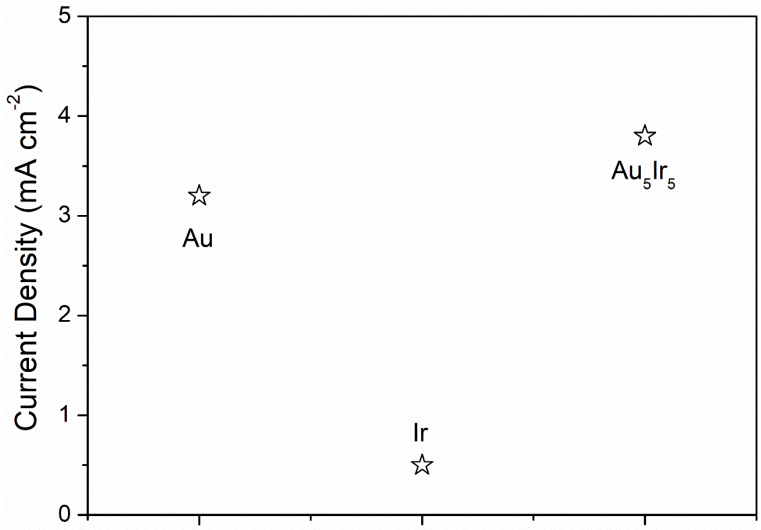

Figure S13 The kinetic currents (j_k) of Au, Au_5Ir_5 alloy and Ir at 0.8 V.

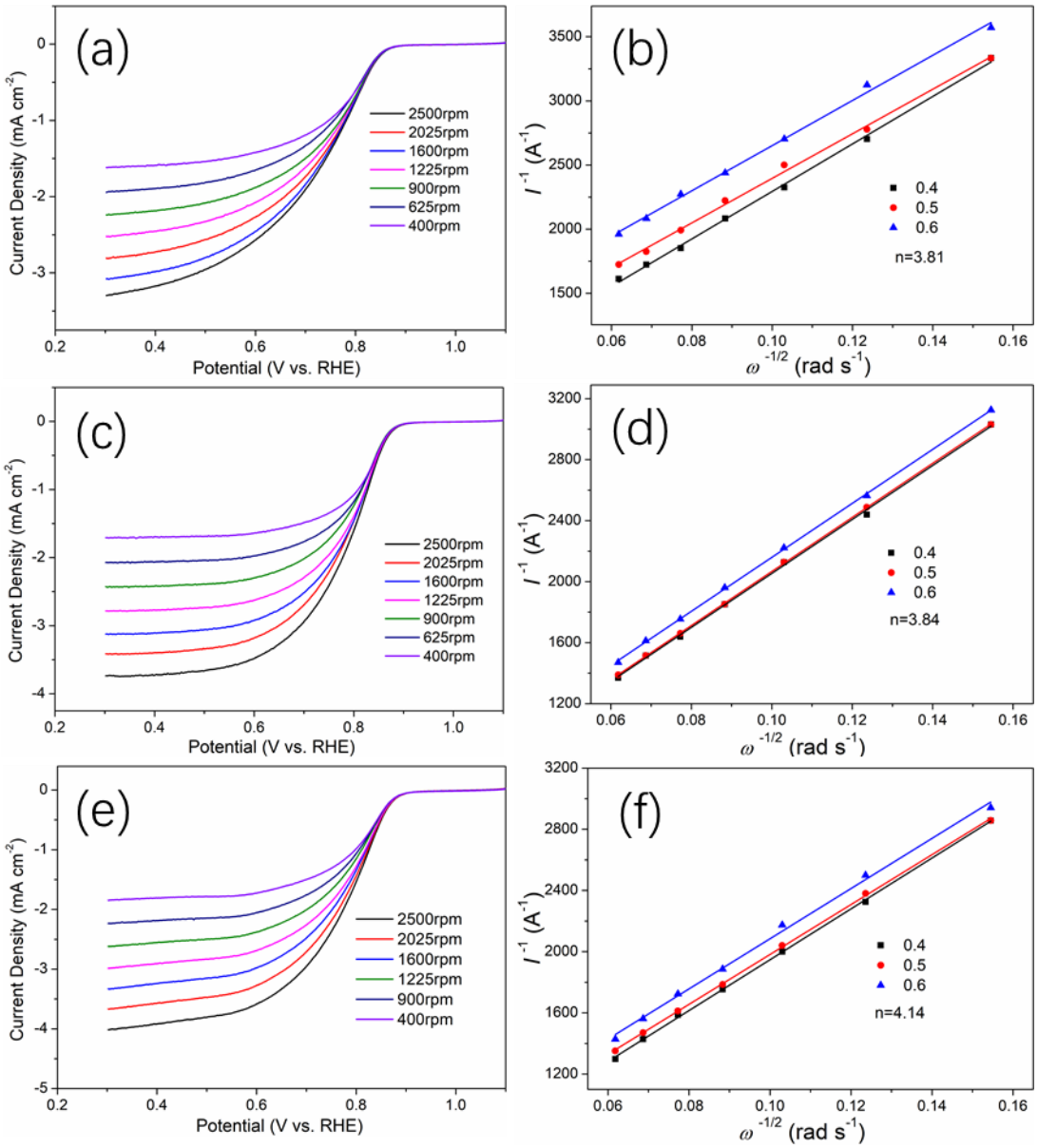

Figure S14 ORR activities at different rotate speeds and transfer electron number (n) under different potential of Au_8Ir_2 alloy (a, b), Au_7Ir_3 alloy (c, d) and Au_3Ir_7 alloy (e, f).

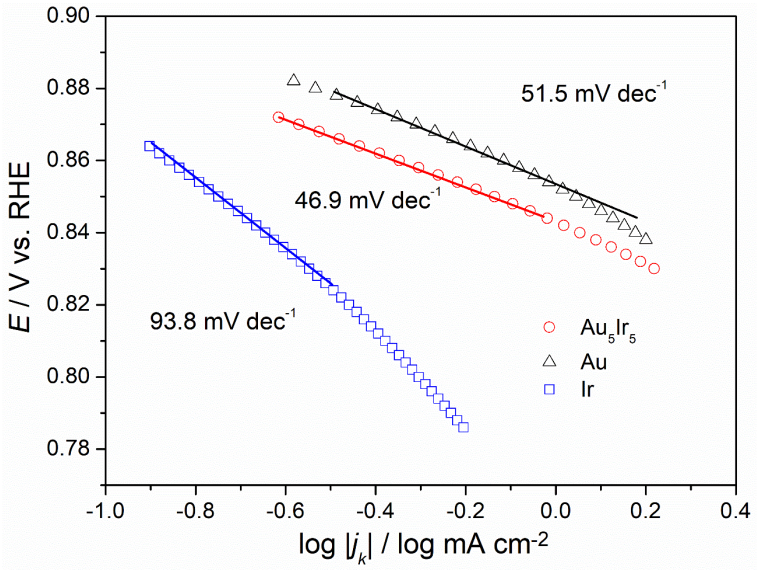

Figure S15 Tafel slopes of Au, Au_5Ir_5 alloy and Ir.

To gain more insights into the reaction kinetics of the ORR, Tafel plots are shown in Fig. S15. The Tafel slope is an indicator of the electrode surface reaction mechanism, which is related to the types of adsorbed oxide species and their corresponding potentials. Generally speaking, a lower Tafel slope means that the adsorption of oxygen and the subsequent reduction reaction proceed more smoothly. The Tafel slope of Au_5Ir_5 is 46.9 mV dec^{-1}, while those of Au and Ir are 51.5 and 93.8 mV dec^{-1}, respectively.

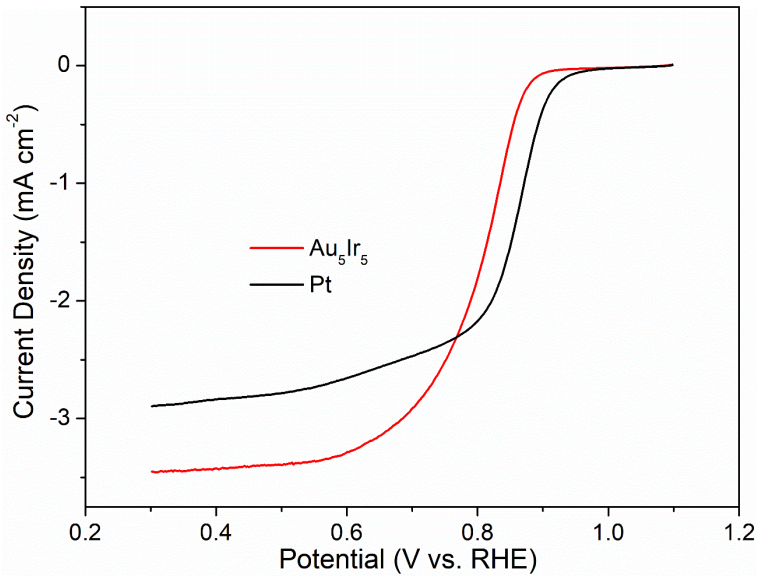

Figure S16 ORR activities of Au_5Ir_5 alloy and Pt.

Unfortunately, the ORR activity of Au_5Ir_5 alloy is still worse than that of Pt (Fig. S16) and needs to be further improved. The limiting current density of Pt is lower than that of Au_5Ir_5, which may be due to its low ECSA.

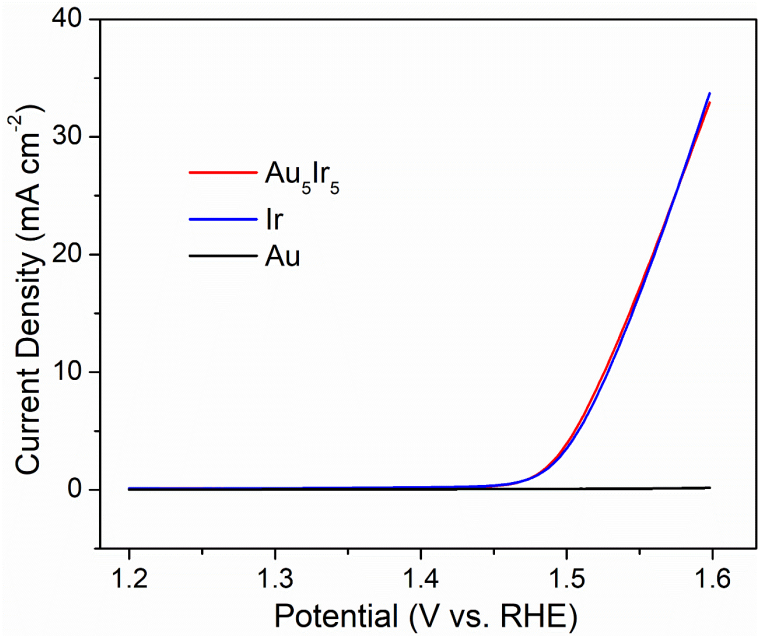

Figure S17 OER activities of Au, Au_5Ir_5 alloy and Ir.

In addition, it is well known that Ir is an excellent oxygen evolution reaction (OER) electrocatalyst. In Fig. S17, the OER activities of Au_5Ir_5 alloy and Ir are the same, indicating that the Au_5Ir_5 alloy has excellent OER activity, although the Ir loading of the Au_5Ir_5 alloy is half of that of pure Ir. The possible reason for this is that when the catalyst loading is high, it has little effect on the OER activity.

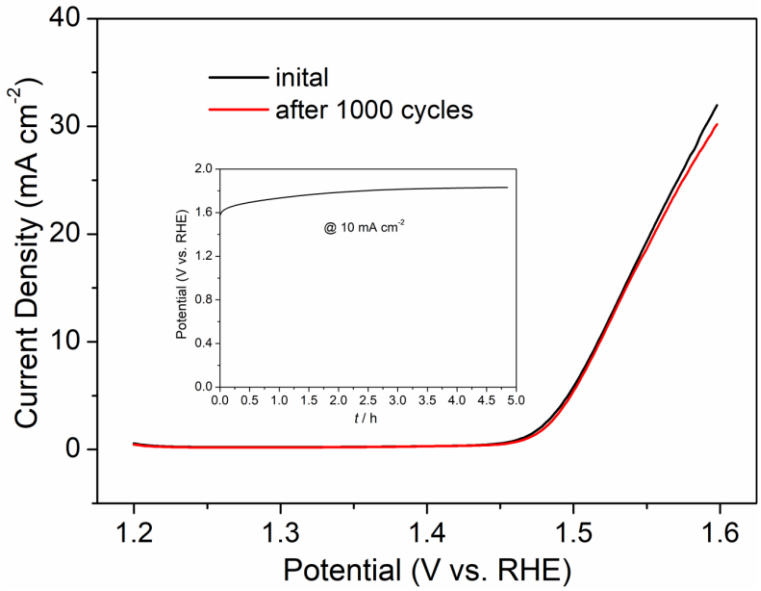

Figure S18 Long-time stability tests of Au_5Ir_5 alloy for OER.

In long-term stability tests, the OER activity of the Au_5Ir_5 catalyst is slightly reduced after 1000 cycle of consecutive CV scans (Fig. S18). Meanwhile, in the chronopotentiometry experiment (I = 10 mA cm^{-2}) (insert in Fig. S18), the stability is not ideal, especially during the initial 2000 s period. The potential increases by 250 mV after 5h. Therefore, the stability should be further improved in future studies.

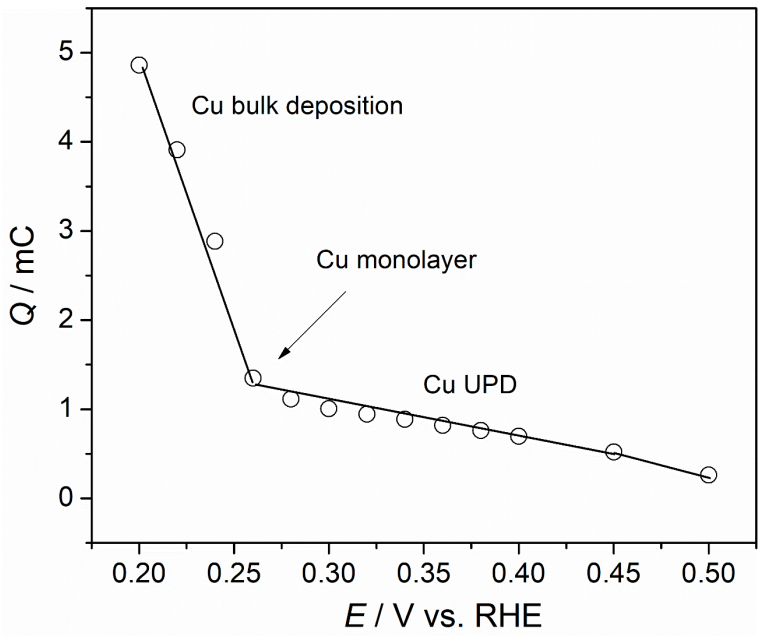

Fig. S19 The oxidation stripping charge (Q) of underpotential deposition of Cu adatoms at different deposition potential (Deposition time = 120 s) in 1.0 mM $CuSO_4$ + 0.1 M H_2SO_4 solution.

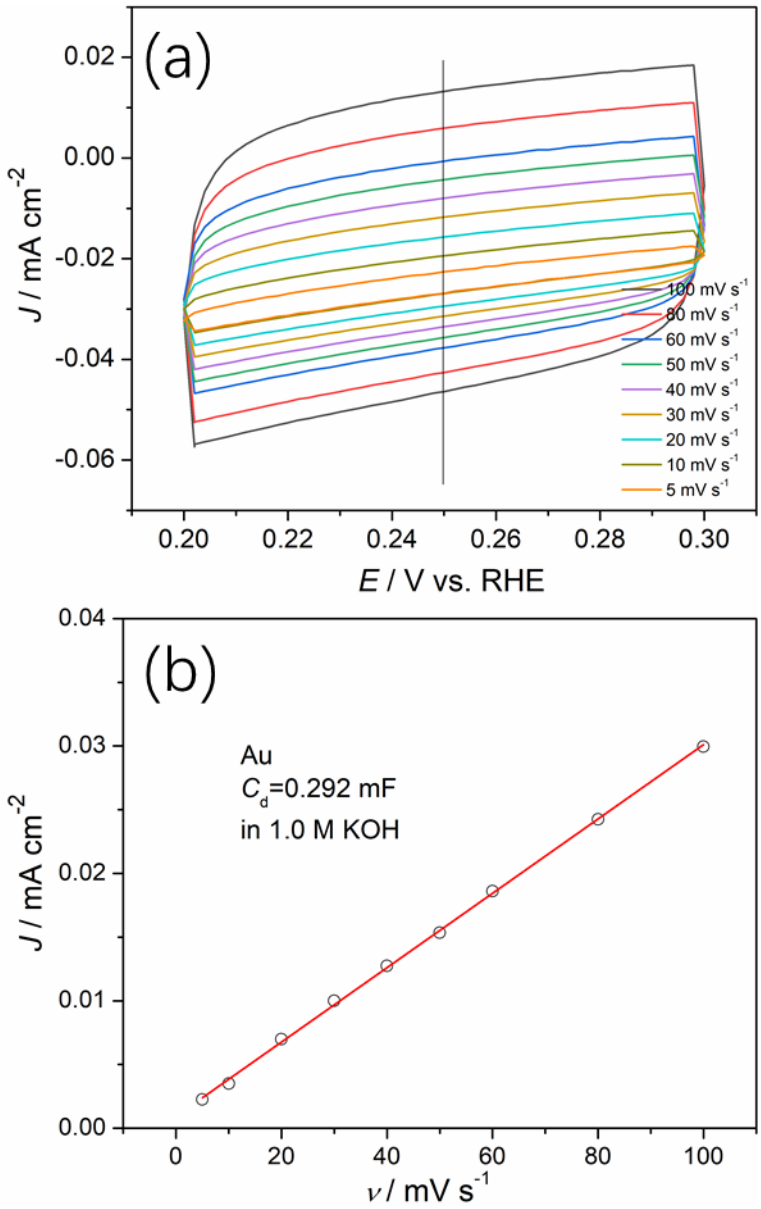

Fig. S20 The double-layer capacitance (C_d) of Au electrode sample (the same sample as Fig. S19) in 1.0 M KOH solution. (a) The double layers at different scanning speeds. (b) The *j* (current of double layer) - *v* (scanning speed) curve.

Table S1 Composition analysis by XRF and loading of AuIr alloy electrodes with different sputtering power and sputtering time

Catalyst	Sputtering power / W		Content / mol%		Sputtering time / min	Loading / mg cm^{-2}
	Au	Ir	Au	Ir		
Au	10	---	100	0	18	0.126
Au_8Ir_2	10	5	80	20	15	0.128
Au_7Ir_3	10	10	65	35	12.5	0.125
Au_5Ir_5[a]	10	30	49	51	8.0	0.125
Au_3Ir_7	10	40	33	67	6.5	0.124
Ir	---	20	0	100	20	0.122

[a]The surface composition analysis by XPS analysis is Au:Ir = 42:58.